

Radar Cross Section of a Terminated, Semi-Infinite Parallel-Plate Waveguide with Material Loading

Shoichi Koshikawa¹⁾ and Kazuya Kobayashi²⁾

¹⁾ R&D Group, Laboratory, Antenna Giken Co., Ltd.

4-72 Miyagayato, Omiya 330-0011, Japan

Tel: +81-48-684-0712, Fax: +81-48-684-9960, E-mail: koshikawa@antenna-giken.co.jp

²⁾ Department of Electrical, Electronic, and Communication Engineering, Chuo University

1-13-27 Kasuga, Bunkyo-ku, Tokyo 112-8551, Japan

Tel: +81-3-3817-1869, Fax: +81-3-3817-1847, E-mail: kazuya@kazuya.elect.chuo-u.ac.jp

The plane wave diffraction by a terminated, semi-infinite parallel-plate waveguide with material loading is rigorously analyzed for both H and E polarizations using the Wiener-Hopf technique. Introducing the Fourier transform for the scattered field and applying boundary conditions in the transform domain, the problem is formulated in terms of the simultaneous Wiener-Hopf equations, which are solved exactly via the factorization and decomposition procedure. The scattered field is evaluated by taking the inverse Fourier transform and applying the saddle point method. Representative numerical examples of the radar cross section (RCS) are given for various physical parameters and the backscattering characteristics are discussed in detail. Some comparisons with a high-frequency technique are also given to validate the present method.

1. Introduction

The analysis of electromagnetic wave scattering from open-ended metallic waveguide cavities has received much attention recently in connection with the prediction and reduction of the radar cross section (RCS) of a target [1, 2]. A number of two- and three-dimensional cavity diffraction problems have been analyzed thus far by means of high-frequency ray techniques and numerical methods [3–10], but it appears that the solutions obtained by these methods are not uniformly valid for arbitrary cavity dimensions.

The Wiener-Hopf technique [11–14] is one of the powerful, rigorous approaches for analyzing wave scattering and diffraction problems associated with canonical geometries. In the previous papers [15–21], we have considered, as an example of simple two-dimensional cavity structures, a finite parallel-plate waveguide with a planar termination at the open end, and analyzed the plane wave diffraction for both empty and material-loaded cases using the Wiener-Hopf technique. As a result, the efficient approximate solution has been obtained, which is valid for cavity depth greater than the incident wavelength. In this paper, as a related two-dimensional geometry, we shall consider a three-layer-loaded cavity formed by a semi-infinite parallel-plate waveguide with an interior planar termination, and analyze the plane wave diffraction rigorously for both H and E polarizations by means of the Wiener-Hopf technique. Introducing the Fourier transform for the unknown scattered field and applying boundary conditions appropriately in the transform domain, the problem is formulated in terms of the simultaneous Wiener-Hopf equations, which are solved exactly in a formal sense via the factorization and decomposition procedure. It should be noted, however, that the formal solution involves infinite series with unknown coefficients. Using the edge condition, we shall further derive approximate expressions of the infinite series, which are then led to the efficient approximate solution of the Wiener-Hopf equations. It is to be noted that our solution is valid for arbitrary cavity dimensions. The scattered field is evaluated by taking the inverse Fourier transform together with the use of the saddle point method. We shall present illustrative numerical examples of the RCS for various physical parameters to discuss the far field backscattering characteristics in detail. It is shown that significant RCS reduction can be

achieved over a broad frequency range by loading the interior of the cavity with three-layer lossy material. Some comparisons with a high-frequency technique are also provided and the validity of that approach is discussed. In the following, the analysis procedure is presented only for the H -polarized case, but numerical results are given for both polarizations.

The time factor is assumed to be $e^{-i\omega t}$ and suppressed throughout this paper.

2. Formulation of the Problem

We consider the diffraction of an H -polarized plane wave by a terminated, semi-infinite parallel-plate waveguide with material loading, as shown in Fig. 1, where the upper and lower plates at $x=\pm b$ and the endplate at $z=-d_1$ are infinitely thin, perfectly conducting, and uniform in the y -direction. The material layers I ($-d_1 < z < -d_2$), II ($-d_2 < z < -d_3$), and III ($-d_3 < z < -d_4$) inside the waveguide are characterized by the relative permittivity/permeability $(\epsilon_{rm}, \mu_{rm})$ for $m=1, 2$, and 3, respectively.

Let the total magnetic field $\phi^t(x, z) [\equiv H_y^t(x, z)]$ be

$$\phi^t(x, z) = \phi^i(x, z) + \phi(x, z), \quad (1)$$

where $\phi^i(x, z)$ is the incident field of H polarization defined by

$$\phi^i(x, z) = e^{-ik(x \sin \theta_0 + z \cos \theta_0)} \quad (2)$$

for $0 < \theta_0 < \pi/2$ with $k = [\omega(\mu_0 \epsilon_0)^{1/2}]$ being the free-space wavenumber. We shall assume that the vacuum is slightly lossy as in $k = k_1 + ik_2$ with $0 < k_2 \ll k_1$. The solution for real k is obtained by letting $k_2 \rightarrow +0$ at the end of analysis. Let us define the Fourier transform of the scattered field in (1) as

$$\Phi(x, \alpha) = (2\pi)^{-1/2} \int_{-\infty}^{\infty} \phi(x, z) e^{i\alpha z} dz, \quad (3)$$

where $\alpha = \text{Re } \alpha + i \text{Im } \alpha (\equiv \sigma + i\tau)$. In view of the radiation condition, it is seen that $\Phi(x, \alpha)$ is regular in the strip $-k_2 < \tau < k_2 \cos \theta_0$ of the complex α -plane. Taking the Fourier transform of the two-dimensional Helmholtz equation and solving the resultant equations, we may derive the scattered field representation in the transform domain as

$$\begin{aligned} \Phi(x, \alpha) &= \mp \gamma^{-1} \Psi'_{(+)}(\pm b, \alpha) e^{-\gamma(x \mp b)} \quad \text{for } x \gtrless \pm b, \\ &= \Psi'_{(+)}(b, \alpha) \frac{\cosh \gamma(x+b)}{\gamma \sinh 2\gamma b} - \Psi'_{(+)}(-b, \alpha) \frac{\cosh \gamma(x-b)}{\gamma \sinh 2\gamma b} \\ &\quad - \frac{1}{b} \sum_{n=0}^{\infty} h_n \left[\frac{c_n(\alpha)}{\alpha^2 + \gamma_n^2} + \sum_{m=1}^3 \frac{c_{mn}(\alpha)}{\alpha^2 + \Gamma_{mn}^2} \right] \cos \frac{n\pi}{2b}(x+b) \quad \text{for } |x| < b, \end{aligned} \quad (4)$$

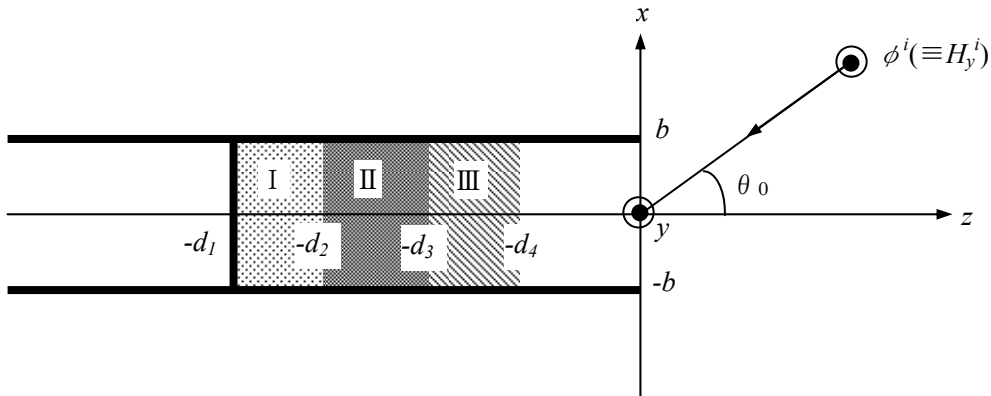


Fig. 1. Geometry of the problem ($-d_1 < -d_2 < -d_3 < -d_4 < 0$).

where $\gamma = (\alpha^2 - k^2)^{1/2}$ with $\text{Re } \gamma > 0$, and

$$\nu_0 = 1/2; \quad \nu_n = 1 \quad \text{for } n \geq 1, \quad (5)$$

$$\gamma_0 = -ik; \quad \gamma_n = [(n\pi/2b)^2 - k^2]^{1/2} \quad \text{for } n \geq 1, \quad (6)$$

$$\Gamma_{m0} = -i(\mu_{rm}\varepsilon_{rm})^{1/2}k; \quad \Gamma_{mn} = [(n\pi/2b)^2 - \mu_{rm}\varepsilon_{rm}k^2]^{1/2} \quad \text{for } n \geq 1 (m=1, 2, 3), \quad (7)$$

$$\Psi'_{(+)}(x, \alpha) = \Phi'_+(x, \alpha) + \frac{k \sin \theta_0 e^{-ik \sin \theta_0}}{(2\pi)^{1/2}(\alpha - k \cos \theta_0)}, \quad (8)$$

$$\Phi'_+(x, \alpha) = (2\pi)^{-1/2} \int_0^\infty \frac{\partial \phi(x, z)}{\partial x} e^{i\alpha z} dz, \quad (9)$$

$$c_n(\alpha) = e^{-i\alpha d_4} (f_{3n}/\varepsilon_{r3} - i\alpha g_{3n}), \quad c_{1n}(\alpha) = -i\alpha e^{-i\alpha d_1} g_n^+ - e^{-i\alpha d_2} (f_{1n} - i\alpha g_{1n}), \quad (10a)$$

$$c_{2n}(\alpha) = e^{-i\alpha d_2} [(\varepsilon_{r2}/\varepsilon_{r1})f_{1n} - i\alpha g_{1n}] - e^{-i\alpha d_3} (f_{2n} - i\alpha g_{2n}), \quad (10b)$$

$$c_{3n}(\alpha) = e^{-i\alpha d_3} [(\varepsilon_{r3}/\varepsilon_{r2})f_{2n} - i\alpha g_{2n}] - e^{-i\alpha d_4} (f_{3n} - i\alpha g_{3n}). \quad (10c)$$

In (10a–c), the coefficients g_n^+ and f_{mn} , g_{mn} for $m=1, 2, 3$ are defined by

$$g_n^+ = -P_n U_{(+)}(i\gamma_n) \quad \text{for } n=1, 3, 5, \dots; = P_n V_{(+)}(i\gamma_n) \quad \text{for } n=0, 2, 4, \dots, \quad (11)$$

$$f_{mn} = -Q_{mn} U_{(+)}(i\gamma_n) \quad \text{for } n=1, 3, 5, \dots; = Q_{mn} V_{(+)}(i\gamma_n) \quad \text{for } n=0, 2, 4, \dots, \quad (12a)$$

$$g_{mn} = -R_{mn} U_{(+)}(i\gamma_n) \quad \text{for } n=1, 3, 5, \dots; = R_{mn} V_{(+)}(i\gamma_n) \quad \text{for } n=0, 2, 4, \dots, \quad (12b)$$

where

$$U_{(+)}(\alpha) = \Psi'_{(+)}(b, \alpha) + \Psi'_{(+)}(-b, \alpha), \quad V_{(+)}(\alpha) = \Psi'_{(+)}(b, \alpha) - \Psi'_{(+)}(-b, \alpha) \quad (13)$$

$$P_n = (1 + \tau_{1n}) e^{-\Gamma_{1n}(d_1-d_2)} Q_{1n}, \quad Q_{1n} = \Gamma_{1n} \tau_{1n} R_{1n}, \quad Q_{2n} = \Gamma_{2n} \tau_{2n} R_{2n}, \quad (14)$$

$$Q_{3n} = \frac{\Gamma_{3n} [1 + \sigma_{2n} e^{-2\Gamma_{3n}(d_3-d_4)}]}{1 - \sigma_{2n} e^{-2\Gamma_{3n}(d_3-d_4)}} R_{3n}, \quad R_{1n} = \frac{(1 - \sigma_{1n})(1 + \tau_{2n}) e^{-\Gamma_{2n}(d_2-d_3)}}{2} R_{2n}, \quad (15)$$

$$R_{2n} = \frac{(1 - \sigma_{2n}) e^{-\Gamma_{3n}(d_3-d_4)}}{1 - \sigma_{2n} e^{-2\Gamma_{3n}(d_3-d_4)}} R_{3n}, \quad R_{3n} = \frac{\varepsilon_{r3} \gamma_n + \Gamma_{3n}}{\varepsilon_{r3} \gamma_n + \Gamma_{3n}} \frac{[1 - \sigma_{2n} e^{-2\Gamma_{3n}(d_3-d_4)}] e^{-\gamma_n d_4}}{1 - \sigma_{2n} \sigma_{3n} e^{-2\Gamma_{3n}(d_3-d_4)}}, \quad (16)$$

$$\sigma_{1n} = \frac{(\varepsilon_{r2}/\varepsilon_{r1})\Gamma_{1n} - \tau_{1n}\Gamma_{2n}}{(\varepsilon_{r2}/\varepsilon_{r1})\Gamma_{1n} + \tau_{1n}\Gamma_{2n}}, \quad \sigma_{2n} = \frac{(\varepsilon_{r3}/\varepsilon_{r2})\Gamma_{2n} - \tau_{2n}\Gamma_{3n}}{(\varepsilon_{r3}/\varepsilon_{r2})\Gamma_{2n} + \tau_{2n}\Gamma_{3n}}, \quad \sigma_{3n} = \frac{\varepsilon_{r3}\gamma_n - \Gamma_{3n}}{\varepsilon_{r3}\gamma_n + \Gamma_{3n}}, \quad (17)$$

$$\tau_{1n} = \frac{1 - e^{-2\Gamma_{1n}(d_1-d_2)}}{1 + e^{-2\Gamma_{1n}(d_1-d_2)}}, \quad \tau_{2n} = \frac{1 - \sigma_{1n} e^{-2\Gamma_{2n}(d_2-d_3)}}{1 + \sigma_{1n} e^{-2\Gamma_{2n}(d_2-d_3)}}. \quad (18)$$

It is noted from (8) and (9) that $\Phi'_+(x, \alpha)$ is regular in $\tau > -k_2$ whereas $\Psi'_{(+)}(x, \alpha)$ is regular in $\tau > -k_2$ except for a simple pole at $\alpha = k \cos \theta_0$. In the following, the subscripts ‘+’ and ‘(+)’ will be adopted for indicating these regularity properties. We shall also use the subscript ‘-’ for functions regular in $\tau < k_2 \cos \theta_0$.

Setting $x = \pm b \pm 0$, $\pm b \mp 0$ in (4) and carrying out some manipulations with the aid of the boundary conditions, we obtain that

$$J_-^d(\alpha) = -\frac{U_{(+)}(\alpha)}{M(\alpha)} - \frac{2}{b} \sum_{n=1, \text{odd}}^\infty \left[\frac{c_n(\alpha)}{\alpha^2 + \gamma_n^2} + \sum_{m=1}^3 \frac{c_{mn}(\alpha)}{\alpha^2 + \Gamma_{mn}^2} \right], \quad (19a)$$

$$J_-^s(\alpha) = -\frac{V_{(+)}(\alpha)}{N(\alpha)} + \frac{2}{b} \sum_{n=0, \text{even}}^\infty v_n \left[\frac{c_n(\alpha)}{\alpha^2 + \gamma_n^2} + \sum_{m=1}^3 \frac{c_{mn}(\alpha)}{\alpha^2 + \Gamma_{mn}^2} \right] \quad (19b)$$

for $-k_2 < \tau < k_2 \cos \theta_0$, where

$$J_-^d(\alpha) = J_-(b, \alpha) - J_-(-b, \alpha), \quad J_-^s(\alpha) = J_-(b, \alpha) + J_-(-b, \alpha), \quad (20)$$

$$J_-(\pm b, \alpha) = \Phi(\pm b \pm 0, \alpha) - \Phi(\pm b \mp 0, \alpha), \quad (21)$$

$$M(\alpha) = \gamma e^{-\gamma b} \cosh \gamma b, \quad N(\alpha) = \gamma e^{-\gamma b} \sinh \gamma b. \quad (22)$$

Equations (19a,b) are the simultaneous Wiener–Hopf equations and can be solved exactly via the factorization and decomposition procedure.

3. Exact Solution

The kernel functions $M(\alpha)$ and $N(\alpha)$ defined by (22) are factorized as [11–14]

$$M(\alpha) = M_+(\alpha)M_-(\alpha), \quad N(\alpha) = N_+(\alpha)N_-(\alpha), \quad (23)$$

where $M_\pm(\alpha)$ and $N_\pm(\alpha)$ are regular and nonzero in $\tau \gtrless \mp k_2$, given by

$$M_+(\alpha) [= M_-(-\alpha)] = (\cos kb)^{1/2} e^{i3\pi/4} (k + \alpha)^{1/2} \exp\{(i\gamma b / \pi) \ln[(\alpha - \gamma) / k]\} \\ \cdot \exp\{(i\alpha b / \pi)[1 - C + \ln(\pi / 2kb) + i\pi / 2]\} \prod_{n=1, \text{odd}}^{\infty} (1 + \alpha / i\gamma_n) e^{2i\alpha b / n\pi}, \quad (24a)$$

$$N_+(\alpha) [= N_-(-\alpha)] = (\sin kb / k)^{1/2} \exp\{(i\gamma b / \pi) \ln[(\alpha - \gamma) / k]\} (1 + \alpha / i\gamma_0) \\ \cdot \exp\{(i\alpha b / \pi)[1 - C + \ln(2\pi / kb) + i\pi / 2]\} \prod_{n=2, \text{even}}^{\infty} (1 + \alpha / i\gamma_n) e^{2i\alpha b / n\pi} \quad (24b)$$

with $C(=0.57721566\dots)$ being Euler's constant. The split functions $M_{\pm}(\alpha)$ and $N_{\pm}(\alpha)$ behave like $O(\alpha^{1/2})$ as $|\alpha| \rightarrow \infty$ with $\tau \gtrless \mp k_2$

We multiply both sides of (19a) and (19b) by $M_-(\alpha)$ and $N_-(\alpha)$, respectively, and apply the decomposition procedure with the aid of the edge condition. After some manipulations, we arrive at

$$U_{(+)}(\alpha) = b^{1/2} M_+(\alpha) \left[-\frac{A}{b(\alpha - k \cos \theta_0)} - \sum_{n=1}^{\infty} \frac{\delta_{2n-1} a_n p_n u_n^+}{b(\alpha + i\gamma_{2n-1})} \right], \quad (25a)$$

$$V_{(+)}(\alpha) = b^{1/2} N_+(\alpha) \left[\frac{B}{b(\alpha - k \cos \theta_0)} - \sum_{n=1}^{\infty} \frac{v_{2n-2} \delta_{2n-2} b_n q_n v_n^+}{b(\alpha + i\gamma_{2n-2})} \right], \quad (25b)$$

where

$$\delta_n = \frac{[\sigma_{2n} e^{-2\Gamma_{3n}(d_3-d_4)} - \sigma_{3n}] e^{-2\gamma_n d_4}}{1 - \sigma_{2n} \sigma_{3n} e^{-2\Gamma_{3n}(d_3-d_4)}}, \quad (26)$$

$$a_n = (bi\gamma_{2n-1})^{-1}, \quad b_n = (bi\gamma_{2n-2})^{-1}, \quad (27)$$

$$p_n = b^{1/2} M_+(i\gamma_{2n-1}), \quad q_n = b^{1/2} N_+(i\gamma_{2n-2}), \quad (28)$$

$$u_n^+ = U_{(+)}(i\gamma_{2n-1}), \quad v_n^+ = V_{(+)}(i\gamma_{2n-2}), \quad (29)$$

$$A = -\left(\frac{2b}{\pi}\right)^{1/2} \frac{k \sin \theta_0 \cos(kb \sin \theta_0)}{M_+(k \cos \theta_0)}, \quad B = -\left(\frac{2b}{\pi}\right)^{1/2} \frac{ik \sin \theta_0 \sin(kb \sin \theta_0)}{N_+(k \cos \theta_0)}. \quad (30)$$

Equations (25a) and (25b) are the exact solutions to the Wiener–Hopf equations (19a) and (19b), respectively, which are uniformly valid for arbitrary cavity dimensions. The unknowns u_n^+ and v_n^+ for $n=1, 2, 3, \dots$ in (25a,b) can be determined with high accuracy by solving appropriate matrix equations numerically.

4. Scattered Field

The Fourier inverse of the scattered field in the transform domain is defined by

$$\phi(x, z) = (2\pi)^{-1/2} \int_{-\infty+ic}^{\infty+ic} \Phi(x, \alpha) e^{-i\alpha z} d\alpha, \quad (31)$$

where $-k_2 < c < k_2 \cos \theta_0$. Substituting the field representation for $|x| < b$ in (4) into (31) and evaluating the resultant integral, we find from (1) that the total field for the region inside the waveguide takes the form

$$\phi'(x, z) = \sum_{n=1}^{\infty} T_{1n} \cosh \Gamma_{1n}(z + d_1) \cos \frac{n\pi}{2b}(x + b) \quad \text{for } -d_1 < z < -d_2, \\ = \sum_{n=1}^{\infty} \left[T_{mn}^- e^{\Gamma_{mn}(z+d_{m+1})} - T_{mn}^+ e^{-\Gamma_{mn}(z+d_{m+1})} \right] \cos \frac{n\pi}{2b}(x + b) \\ \text{for } -d_m < z < -d_{m+1} (m = 2, 3), \\ = \sum_{n=1}^{\infty} \left[T_{0n}^- e^{\gamma_n(z+d_4)} - T_{0n}^+ e^{-\gamma_n(z+d_4)} \right] \cos \frac{n\pi}{2b}(x + b) \quad \text{for } -d_4 < z < 0,$$

where

$$T_{1n} = -2K_{1n} P_n \Gamma_{1n} U_{(+)}(i\gamma_n) \quad \text{for } n = 1, 3, 5, \dots, \\ = 2K_{1n} P_n \Gamma_{1n} V_{(+)}(i\gamma_n) \quad \text{for } n = 0, 2, 4, \dots, \quad (33)$$

$$\begin{aligned} T_{mn}^{\pm} &= -K_{mn} S_{mn}^{\mp} U_{(+)}(i\gamma_n) \quad \text{for } n=1, 3, 5, \dots (m=2, 3), \\ &= K_{mn} S_{mn}^{\mp} V_{(+)}(i\gamma_n) \quad \text{for } n=0, 2, 4, \dots (m=2, 3), \end{aligned} \quad (34)$$

$$\begin{aligned} T_{0n}^{+} &= -e^{\gamma_n d_4} \kappa_n \delta_n U_{(+)}(i\gamma_n) \quad \text{for } n=1, 3, 5, \dots, \\ &= e^{\gamma_n d_4} \kappa_n \delta_n V_{(+)}(i\gamma_n) \quad \text{for } n=0, 2, 4, \dots, \end{aligned} \quad (35a)$$

$$\begin{aligned} T_{0n}^{-} &= -e^{-\gamma_n d_4} \kappa_n U_{(+)}(i\gamma_n) \quad \text{for } n=1, 3, 5, \dots, \\ &= e^{-\gamma_n d_4} \kappa_n V_{(+)}(i\gamma_n) \quad \text{for } n=0, 2, 4, \dots, \end{aligned} \quad (35b)$$

$$K_{mn} = v_n (\pi/2)^{1/2} / b \Gamma_{mn}, \quad m=1, 2, 3, \quad \kappa_n = v_n (1/2)^{1/2} / b \gamma_n, \quad (36)$$

$$S_{mn}^{\pm} = Q_{mn} \mp \Gamma_{mn} R_{mn}, \quad m=2, 3. \quad (37)$$

Next we shall consider the field outside the waveguide and derive the scattered far field. The region outside the waveguide actually includes $z > 0$ with $|x| < b$, but this region is of less interest in the far field from a practical point of view. Therefore, the derivation of the scattered far field only for $|x| > b$ will be discussed in the following. In view of (4) and (31), an integral representation of the scattered field for $x \gtrless \pm b$ is given by

$$\phi(x, z) = (2\pi)^{-1/2} \int_{-\infty+ic}^{\infty+ic} \gamma^{-1} \Psi'_{(+)}(\pm b, \alpha) e^{\mp \gamma(x \mp b) - i\alpha z} d\alpha, \quad (38)$$

where $\Psi'_{(+)}(\pm b, \alpha)$ is expressed using (13) as

$$\Psi'_{(+)}(\pm b, \alpha) = (1/2) [U_{(+)}(\alpha) \pm V_{(+)}(\alpha)]. \quad (39)$$

It is noted from (25a,b) and (39) that $\Psi'_{(+)}(\pm b, \alpha)$ have a simple pole at $\alpha = k \cos \theta_0$. In order to evaluate (38), we express $\phi(x, z)$ as in

$$\phi(x, z) = \phi_1(x, z) + \phi_2(x, z), \quad (40)$$

where

$$\phi_1(x, z) = \mp (2\pi)^{-1/2} \int_{-\infty+ic}^{\infty+ic} \gamma^{-1} [\Psi_{(+)}(\pm b, \alpha) - \tilde{\Phi}(\pm b, \alpha)] e^{\mp \gamma(x \mp b) - i\alpha z} d\alpha, \quad (41)$$

$$\phi_2(x, z) = \mp (2\pi)^{-1/2} \int_{-\infty+ic}^{\infty+ic} \gamma^{-1} \tilde{\Phi}(\pm b, \alpha) e^{\mp \gamma(x \mp b) - i\alpha z} d\alpha \quad (42)$$

for $x \gtrless \pm b$ with

$$\tilde{\Phi}(\pm b, \alpha) = \frac{k \sin \theta_0 e^{\mp ikb \sin \theta_0} (k + k \cos \theta_0)^{1/2}}{(2\pi)^{1/2} (\alpha + k)^{1/2} (\alpha - k \cos \theta_0)}. \quad (43)$$

Let us introduce the cylindrical coordinates $(\rho_{1,2}, \theta_{1,2})$ centered at the waveguide edges $(x, z) = (\pm b, 0)$ as follows:

$$x - b = \rho_1 \sin \theta_1, \quad z = \rho_1 \cos \theta_1 \quad \text{for } 0 < \theta_1 < \pi, \quad (44a)$$

$$x + b = \rho_2 \sin \theta_2, \quad z = \rho_2 \cos \theta_2 \quad \text{for } -\pi < \theta_2 < 0. \quad (44b)$$

Applying the saddle point method, $\phi_1(x, z)$ defined by (41) can be expanded asymptotically with the result that

$$\phi_1(\rho_{1,2}, \theta_{1,2}) \square \pm [\Psi'_{(+)}(\pm b, -k \cos \theta_{1,2}) - \tilde{\Phi}(\pm b, -k \cos \theta_{1,2})] \frac{e^{i(k\rho_{1,2} - 3\pi/4)}}{(k\rho_{1,2})^{1/2}} \quad (45)$$

for $x \gtrless \pm b$ as $k\rho_{1,2} \rightarrow \infty$. The term $\phi_2(x, z)$ given by (42) is evaluated exactly as in

$$\begin{aligned} \phi_2(\rho_{1,2}, \theta_{1,2}) &= -e^{\mp ikb \sin \theta_0} \left(e^{-ik\rho_{1,2} \cos(\theta_{1,2} - \theta_0)} F\{(2k\rho_{1,2})^{1/2} \cos[(\theta_{1,2} - \theta_0)/2]\} \right. \\ &\quad \left. - e^{-ik\rho_{1,2} \cos(\theta_{1,2} + \theta_0)} F\{(2k\rho_{1,2})^{1/2} \cos[(\theta_{1,2} + \theta_0)/2]\} \right) \end{aligned} \quad (46)$$

for $x \gtrless \pm b$, where $F(\cdot)$ is the Fresnel integral defined by

$$F(w) = \frac{e^{-i\pi/4}}{\pi^{1/2}} \int_w^{\infty} e^{it^2} dt. \quad (47)$$

Therefore, substituting (45) and (46) into (40) yields the scattered far field expression that

holds uniformly in observation angles $\theta_{1,2}$.

Introducing the cylindrical coordinate (ρ, θ) as $x = \rho \sin \theta$, $z = \rho \cos \theta$ for $-\pi < \theta < \pi$, it is seen that the following approximate relationship holds in the far field:

$$\cos \theta_1 \approx \cos \theta \approx \cos \theta_2, \quad (48a)$$

$$\rho \approx \rho_1 + b \sin \theta \quad \text{for } 0 < \theta < \pi; \quad \rho \approx \rho_2 - b \sin \theta \quad \text{for } -\pi < \theta < 0. \quad (48b)$$

Replacing the Fresnel integrals in (46) by their asymptotic expansions for large $|k|\rho_{1,2}$ and using (48a,b), we can show from (40), (45), and (46) that an alternative expression for the scattered far field is

$$\phi(\rho, \theta) \approx \phi^g(\rho, \theta) + \phi^d(\rho, \theta), \quad \theta_{1,2} \approx \pm \pi \mp \theta_0, \quad (49)$$

where $\phi^g(\rho, \theta)$ and $\phi^d(\rho, \theta)$ denote the geometrical optics field and the diffracted field, respectively, given by

$$\begin{aligned} \phi^g(\rho, \theta) &= -e^{-ik\rho \cos(\theta - \theta_0)} \quad \text{for } -\pi < \theta_2 < -\pi + \theta_0, \\ &= 0 \quad \text{for } -\pi + \theta_0 < \theta_2 < 0, \quad 0 < \theta_1 < \pi - \theta_0, \\ &= e^{-2ikb \sin \theta_0} e^{-ik\rho \cos(\theta + \theta_0)} \quad \text{for } \pi - \theta_0 < \theta_1 < \pi, \end{aligned} \quad (50)$$

$$\phi^d(\rho, \theta) = \pm \Psi'_{(+)}(\pm b, -k \cos \theta) e^{\mp ikb \sin \theta} \frac{e^{i(k\rho - 3\pi/4)}}{(k\rho)^{1/2}} \quad \text{for } \theta \gtrless 0. \quad (51)$$

The analysis has thus far been carried out by assuming $0 < \theta_0 < \pi/2$, but the results are in fact true for arbitrary θ_0 .

5. Numerical Results and Discussion

In this section, we shall present numerical examples of the RCS for both H and E polarizations to discuss the far field backscattering characteristics in detail. The normalized RCS per unit length is defined by

$$\frac{\sigma}{\lambda} = \lim_{\rho \rightarrow \infty} \left(k\rho \frac{|\phi^d|^2}{|\phi^i|^2} \right) \quad (52)$$

with λ being the free-space wavelength, where $|\phi^i| = 1$ in view of (2), and ϕ^d is the diffracted field defined by (51) for the H polarization. The definition of the diffracted field ϕ^d for the E -polarized case is omitted.

Figures 2 and 3 show numerical results of the monostatic RCS as a function of incidence angle θ_0 for H and E polarizations, respectively. In numerical computations, cavity dimensions have been taken as $kb = 3.14, 15.7, 31.4$ with $d_1/2b = 1.0$. We have chosen Emerson & Cuming AN-73 [1], where the material constants are $\varepsilon_{r1} = 3.4 + i0.0$, $\varepsilon_{r2} = 1.6 + i0.9$, $\varepsilon_{r3} = 1.4 + i0.35$, $\mu_{r1} = \mu_{r2} = \mu_{r3} = 1.0$, and the thickness of each layer is such that $d_1 - d_2 = d_2 - d_3 = d_3 - d_4 = (t/3)$ (see Fig. 1). In order to investigate the effect of multilayer material loading, we have also computed the RCS for the single-layer case with $\varepsilon_{r1} = \varepsilon_{r2} = \varepsilon_{r3} = 1.4 + i0.35$, $\mu_{r1} = \mu_{r2} = \mu_{r3} = 1.0$, $d_1 - d_4 = t$. The thickness of the single- and three-layer materials is taken as $kt = 2.08$.

It is seen from the figure that, for empty cavities, the RCS exhibits large values over some range due to the effect of interior irradiation, whereas the irradiation is reduced for the case of material loading. Comparing the results of empty cavities, we notice that if the cavity dimension is small ($kb = 3.14$), there are great differences depending on the incident polarization whereas the RCS for both polarizations shows close features with an increase of the cavity dimension. For loaded cavities, we find by comparing the characteristics for the single- and three-layer cases in Figs. 2 and 3 that the RCS reduction is noticeable in the three-layer case.

From the figure, it is also seen that the effect of the three-layer loading is more significant in the H polarization than in the E polarization.

We shall now investigate the frequency dependences of the RCS to make a more detailed consideration on the RCS reduction characteristics. Figure 4 shows the monostatic RCS as a function of normalized frequency kb with $\theta_0 = 10^\circ$, $d_1/2b = 1.0$, where three different cavity geometries are again considered, namely, an empty cavity and cavities with single- and three-layer loading. For loaded cavities, the material-layer parameters are the same as in Figs. 2 and 3. We observe from the results for empty cavities that the average RCS level becomes large with an increase of kb , whereas the RCS is reduced for loaded cavities over the whole frequency range shown in the figure. On comparing the characteristics for the single- and three-layer loading, the RCS reduction is significant in the three-layer case. Therefore, it is confirmed that multilayer lossy materials can be used as broadband absorbing structures. We also notice by comparing with the results for the E -polarized case that the better RCS reduction is achieved in the H polarization.

Finally we shall make some comparisons with the results based on a high-frequency technique. In Figs. 5 and 6, the present Wiener–Hopf solution is compared with the results generated by Burkholder [22] using the hybrid asymptotic-modal approach [6], where solid lines and dots denote the Wiener–Hopf results and Burkholder's results, respectively. It is seen from the figure that the agreement between the two methods is excellent for $0^\circ < \theta_0 < 65^\circ$ whereas there are discrepancies near $\theta_0 = 80^\circ$. In the hybrid asymptotic-modal approach, the external scattering from the leading edges is determined via the use of the first order diffraction coefficient in the geometrical theory of diffraction. The discrepancies for large θ_0 are perhaps due to the fact that the effect of higher order diffraction by the outer edges is not incorporated into Burkholder's analysis.

6. Conclusions

In this paper, we have considered a terminated, semi-infinite parallel-plate waveguide with three-layer material loading, and analyzed rigorously the plane wave diffraction for both H and E polarizations using the Wiener–Hopf technique. It is to be noted that the final solution obtained here is rigorous and uniformly valid for arbitrary cavity dimensions. We have presented numerical examples of the monostatic RCS for various physical parameters to discuss the far field backscattering characteristics in detail. In particular, it has been clarified that multilayer lossy materials play an important role in the RCS reduction over a broad frequency range. Some comparisons with a high-frequency technique have been provided and the validity of that approach has been discussed. The results obtained in this paper can be used as a reference solution for validating more general-purpose computer codes based on approximate methods.

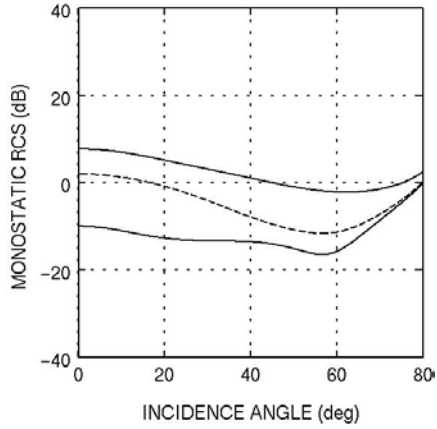
Acknowledgments

The authors would like to thank Dr. Robert J. Burkholder of The Ohio State University for providing the numerical data in Fig. 4. This work was supported in part by the Institute of Science and Engineering, Chuo University.

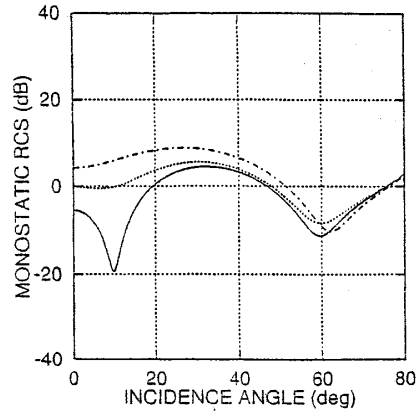
References

- [1] S.-W. Lee and H. Ling, "Data book for cavity RCS: Version 1," *Tech. Rep.*, no. SWL 89-1, Univ. Illinois, Urbana, January 1989.
- [2] W. R. Stone, Ed., *Radar Cross Sections of Complex Objects*, IEEE Press, New York, 1990.
- [3] C. S. Lee and S.-W. Lee, "RCS of a coated circular waveguide terminated by a perfect conductor," *IEEE Trans. Antennas Propagat.*, vol. AP-35, no. 4, pp. 391–398, April 1987.
- [4] A. Altıntaş, P. H. Pathak, and M. C. Liang, "A selective modal scheme for the analysis of EM coupling into or radiation from large open-ended waveguides," *IEEE Trans. Antennas Propagat.*,

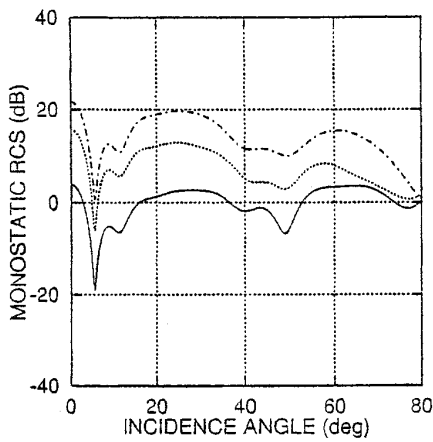
- vol. AP-36, no. 1, pp. 84–96, January 1988.
- [5] H. Ling, R.-C. Chou, and S.-W. Lee, "Shooting and bouncing rays: calculating the RCS of an arbitrary shaped cavity," *IEEE Trans. Antennas Propagat.*, vol. AP-37, no. 2, pp. 194–205, February 1989.
 - [6] P. H. Pathak and R. J. Burkholder, "Modal, ray, and beam techniques for analyzing the EM scattering by open-ended waveguide cavities," *IEEE Trans. Antennas Propagat.*, vol. AP-37, no. 5, pp. 635–647, May 1989.
 - [7] S.-K. Jeng, "Scattering from a cavity-backed slit in a ground plane — TE case," *IEEE Trans. Antennas Propagat.*, vol. AP-38, no. 10, pp. 1523–1529, October 1990.
 - [8] T.-M. Wang and H. Ling, "A connection algorithm on the problem of EM scattering from arbitrary cavities," *J. Electromagn. Waves Appl.*, vol. 5, no. 3, pp. 301–314, 1991.
 - [9] R. Lee and T.-T. Chia, "Analysis of electromagnetic scattering from a cavity with a complex termination by means of a hybrid ray-FDTD method," *IEEE Trans. Antennas Propagat.*, vol. AP-41, no. 11, pp. 1560–1569, November 1993.
 - [10] S. Ohnuki and T. Hinata, "Radar cross section of an open-ended rectangular cylinder with an iris inside the cavity," *IEICE Trans. Electron.*, vol. E81-C, no. 12, pp. 1875–1880, December 1998.
 - [11] B. Noble, *Methods Based on the Wiener–Hopf Technique for the Solution of Partial Differential Equations*, Pergamon Press, London, 1958.
 - [12] R. Mittra and S.-W. Lee, *Analytical Techniques in the Theory of Guided Waves*, Macmillan, New York, 1971.
 - [13] K. Kobayashi, "The Wiener–Hopf technique with applications to scattering and diffraction problems," in *A Course of Applied Mathematics*, Chap. 9 (in Japanese), Horiuchi, K., Ed., Corona Publishing, Tokyo, 1989.
 - [14] K. Kobayashi, "Wiener–Hopf and modified residue calculus techniques," in *Analysis Methods for Electromagnetic Wave Problems*, Chap. 8, Yamashita, E., Ed., Artech House, Boston, 1990.
 - [15] K. Kobayashi and A. Sawai, "Plane wave diffraction by an open-ended parallel plate waveguide cavity," *J. Electromagn. Waves Appl.*, vol. 6, no. 4, pp. 475–512, 1992.
 - [16] S. Koshikawa and K. Kobayashi, "Diffraction by a parallel-plate waveguide cavity with a thick planar termination," *IEICE Trans. Electron.*, vol. E76-C, no. 1, pp. 142–158, January 1993.
 - [17] K. Kobayashi, S. Koshikawa, and A. Sawai, "Diffraction by a parallel-plate waveguide cavity with dielectric/ferrite loading: Part I – The case of E polarization," in *Progress in Electromagnetics Research*, PIER 8, Chap. IX, J. A. Kong, Ed., EMW Publishing, Cambridge, 1994.
 - [18] S. Koshikawa and K. Kobayashi, "Diffraction by a parallel-plate waveguide cavity with dielectric/ferrite loading: Part II – The case of H polarization," in *Progress in Electromagnetics Research*, PIER 8, Chap. X, J. A. Kong, Ed., EMW Publishing, Cambridge, 1994.
 - [19] S. Koshikawa and K. Kobayashi, "Wiener–Hopf analysis of the diffraction by a parallel-plate waveguide cavity with partial material loading," *IEICE Trans. Electron.*, vol. E77-C, no. 6, pp. 975–985, June 1994.
 - [20] S. Koshikawa, T. Momose, and K. Kobayashi, "RCS of a parallel-plate waveguide cavity with three-layer material loading," *IEICE Trans. Electron.*, vol. E77-C, no. 9, pp. 1514–1521, September 1994.
 - [21] S. Koshikawa, D. Çolak, A. Altıntaş, K. Kobayashi, and A. I. Nosich, "A comparative study of RCS predictions of canonical rectangular and circular cavities with double-layer material loading," *IEICE Trans. Electron.*, vol. E80-C, no. 11, pp. 1457–1466, November 1997.
 - [22] R. J. Burkholder, private communication, July 1993.



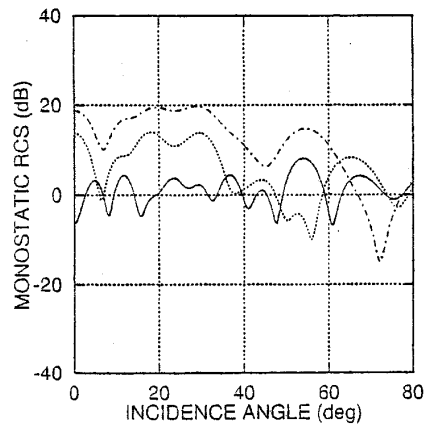
(a) $kb = 3.14$.



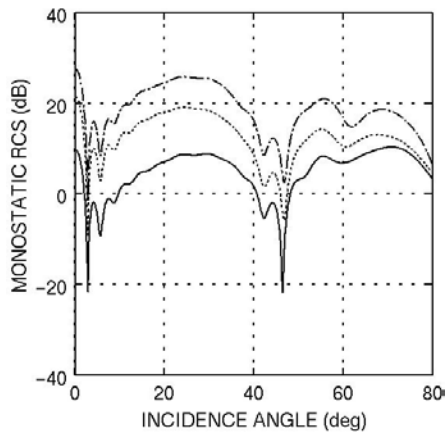
(a) $kb = 3.14$.



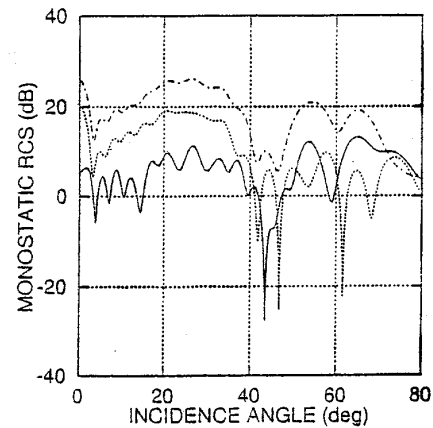
(b) $kb = 15.7$.



(b) $kb = 15.7$.



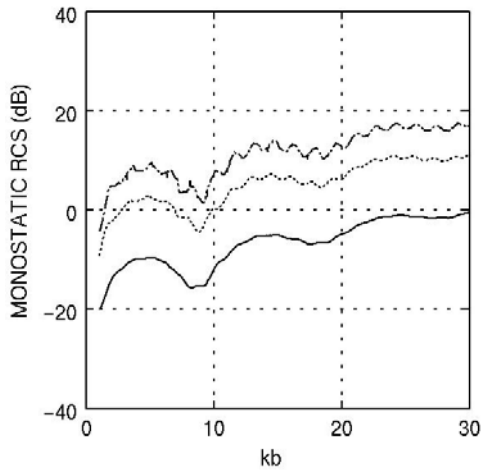
(c) $kb = 31.4$.



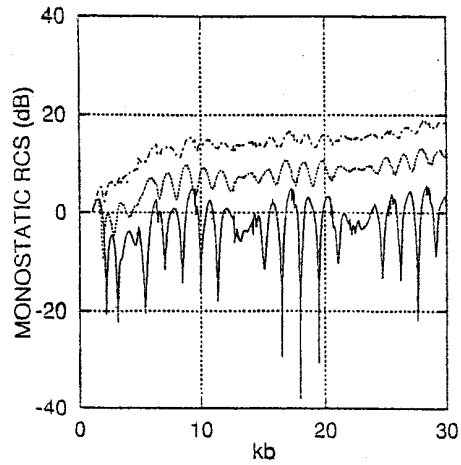
(c) $kb = 31.4$.

Fig. 2. Monostatic RCS σ/λ [dB] versus incidence angle θ_0 for H polarization, $d_1/2b=1.0$. - - - - : empty; : single-layer loading with $\epsilon_{r1} = \epsilon_{r2} = \epsilon_{r3} = 1.4 + i0.35$, $\mu_{r1} = \mu_{r2} = \mu_{r3} = 1.0$, $kt = 2.08$; _____ : three-layer loading with Emerson & Cuming AN-73, $kt = 2.08$.

Fig. 3. Monostatic RCS σ/λ [dB] versus incidence angle θ_0 for E polarization, $d_1/2b=1.0$. - - - - : empty; : single-layer loading with $\epsilon_{r1} = \epsilon_{r2} = \epsilon_{r3} = 1.4 + i0.35$, $\mu_{r1} = \mu_{r2} = \mu_{r3} = 1.0$, $kt = 2.08$; _____ : three-layer loading with Emerson & Cuming AN-73, $kt = 2.08$.

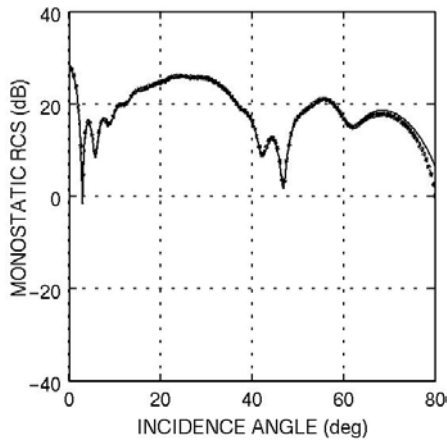


(a) H polarization.

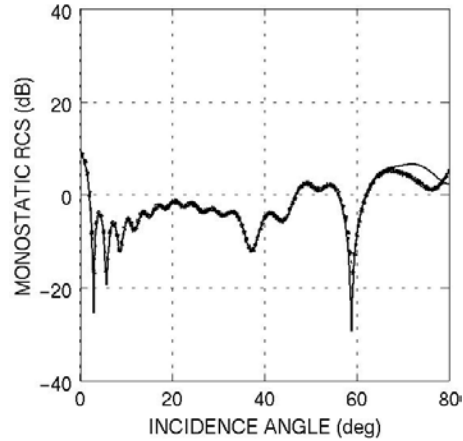


(b) E polarization

Fig. 4. Monostatic RCS σ/λ [dB] versus normalized frequency kb for $\theta_0 = 10^\circ$, $d_1/2b = 1.0$. - - - - : empty; : single-layer loading with $\epsilon_{r1} = \epsilon_{r2} = \epsilon_{r3} = 1.4 + i0.35$, $\mu_{r1} = \mu_{r2} = \mu_{r3} = 1.0$, $kt = 2.08$; ———: three-layer loading with Emerson & Cuming AN-73, $kt = 2.08$.

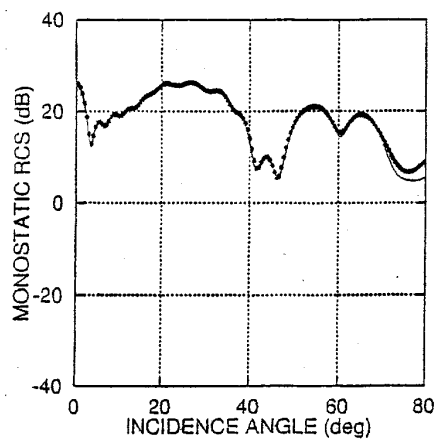


(a) $t = 0$.

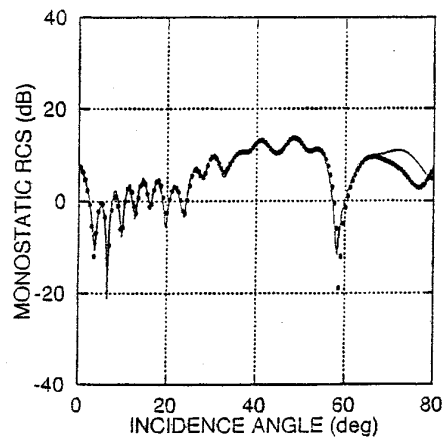


(b) $t = d_1/2$.

Fig. 5. Monostatic RCS σ/λ [dB] versus incidence angle θ_0 for H polarization, $d_1/2b = 1.0$, $2b = 10\lambda$, $\epsilon_{r1} = \epsilon_{r2} = \epsilon_{r3} = 2.5 + i1.25$, $\mu_{r1} = \mu_{r2} = \mu_{r3} = 1.6 + i0.8$ and its comparison with Burkholder [22]. Solid lines and dots denote the results of this paper and Burkholder's results, respectively.



(a) $t = 0$.



(b) $t = d_1/2$.

Fig. 6. Monostatic RCS σ/λ [dB] versus incidence angle θ_0 for E polarization, $d_1/2b = 1.0$, $2b = 10\lambda$, $\epsilon_{r1} = \epsilon_{r2} = \epsilon_{r3} = 2.5 + i1.25$, $\mu_{r1} = \mu_{r2} = \mu_{r3} = 1.6 + i0.8$ and its comparison with Burkholder [22]. Solid lines and dots denote the results of this paper and Burkholder's results, respectively.